Limnol. Oceanogr., 47(2), 2002, 535–544

Observations of mixing near the sides of a deep lake in winter

Ilker Fer[1] *and Ulrich Lemmin*
Laboratoire de Recherches Hydrauliques, Dépt. Génie Civil, Ecole Polytechnique Fédérale de Lausanne, CH-1015 Lausanne, Switzerland

S. A. Thorpe
School of Ocean and Earth Science, Southampton Oceanography Centre, European Way, Southampton SO14 3ZH, United Kingdom

Abstract

The dissipation rate of turbulent kinetic energy per unit mass, ε, vertical eddy diffusivity, K_z, and the rate of dissipation of temperature variance, χ, are estimated over the sloping sides of Lake Geneva both far from and near the bed, using temperature data from horizontal tracks of a submarine during periods of winter cooling. The estimated values are about one order of magnitude greater near the slope than those distant from it. The mean dissipation rate per unit mass averaged over the epilimnion varies between $O(10^{-10})$ m^2 s^{-3} in calm weather to $O(10^{-8})$ m^2 s^{-3} in winds of 8 m s^{-1}, for surface buoyancy fluxes of 6×10^{-9} m^2 s^{-3} and 1.1×10^{-8} m^2 s^{-3}, whereas near the slope ε has an average value of 3×10^{-8} m^2 s^{-3}. The relation between K_z and εN^{-2} (where N is the buoyancy frequency) is examined. Values of the mixing efficiency, $\Gamma = \varepsilon N^{-2} K_z^{-1}$, of 0.15 ± 0.1 and 0.16 ± 0.1 are obtained in the upper 10-m layer for calm and windy conditions, respectively. Near the slope, Γ is found to be 0.22 ± 0.2, slightly larger than in surface layers under windy conditions. Different mixing mechanisms in different regions, near the slope and in the surface waters of the epilimnion and relatively calm deeper layers, can be identified in the diagram of overturn Froude number versus overturn Reynolds number. Mixing near the slope in the epilimnion appears to be related to the gravitational winter cascading of cold water down the sloping sides of the lake.

It is known from measurements that mixing is often more intense in the vicinity of sloping boundaries in the stratified ocean (Thorpe et al. 1990; Van Haren et al. 1994; Ledwell and Hickey 1995; Polzin et al. 1997; Toole et al. 1997; Ledwell et al. 2000) and in lakes (Imberger and Ivey 1991, 1993; Wüest et al. 1996; Goudsmit et al. 1997; MacIntyre et al. 1999). This difference can frequently be ascribed to the effects of the interaction of along-slope currents or internal waves with the topography, including wave reflection and wave breaking, which may be more intense near critical slopes (Eriksen 1998).

Here we investigate boundary-mixing dynamics in a lake during a period of winter cooling and weak stratification. A study was made near the northern shore of Lake Geneva using a small submarine operating in the epilimnion. Data from an array of six fast-response thermistors mounted on the bow are used to investigate and contrast the nature of small-scale temperature variability in midwater and near the sloping boundary of the lake, down which a cold density current flows as a result of cooling at the lake surface. Three parameters are derived to characterize mixing: the rate of dissipation of turbulent kinetic energy per unit mass ε, the rate of dissipation of temperature variance χ, and the vertical eddy diffusivity of heat K_z. These are estimated from the temperature fluctuation and temperature fluctuation gradient spectra (Gibson and Schwarz 1963) and the equation for diffusivity derived by Osborn and Cox (1972).

Location and the submarine

The observations are part of a study of the dynamical effects of winter cooling. They were made in the vicinity of Ouchy (46°31′N, 6°36′E), on the northern shore of Lake Geneva, which is about 70 km long. Here in the central part of the lake basin, the lake is 12 km wide. Close to shore, the depth increases gradually to about 4 m over a region some 100 m wide. The sides then slope down at about 10° to a central plateau at 310-m depth. Figure 1 shows the bathymetry of the area.

For the present study, the three-man submarine, *F.A. Forel,* was equipped with a vertical array of six high-precision temperature sensors spanning a maximum vertical length of 1.68 m. They are mounted on rods protruding horizontally 0.53 m ahead of a vertical spar, which is supported on a frame and is carried about 2.5 m in front of the bow of the 2.2-m wide submarine (Thorpe et al. 1999). The sensors built by Precision Measurement Techniques have a time response of 20 ms and record to 1×10^{-3} °C resolution at frequencies of up to 30 Hz. They were calibrated in the laboratory prior to the dives. Small shifts, about 3 mK from the mean trend, were found, and the data were corrected accordingly.

Depth (via pressure) and two tilt (roll and pitch) and compass (heading) angles are recorded in parallel to the temperature data to 0.1 m and 1° resolution, respectively. The sensors were in a housing placed on the deck of the submarine (~10 cm above deck level). The submarine is connected by

[1] Current address: Geophysical Institute, University of Bergen, Allegaten 70, N-5007, Bergen, Norway.

Acknowledgments

We thank Dr. J. Piccard and his sponsors for use of the submarine, *F.A. Forel.* Financial support for this project is provided by the Swiss Science Foundation, grant 20-49502.96. The constructive comments of the anonymous reviewers and their assistance in evaluating the paper are appreciated.

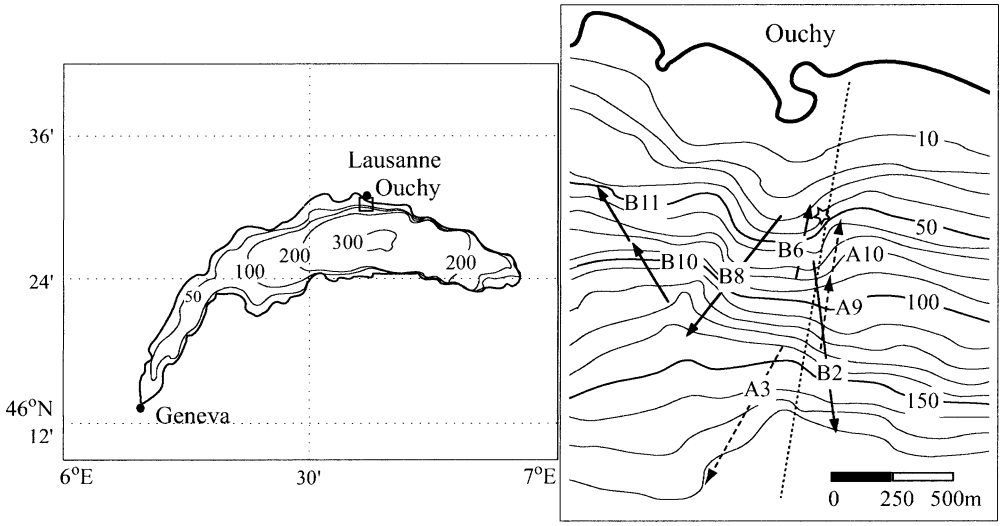

Fig. 1. The bathymetric map of Lake Geneva with an inset of the observation area, Ouchy (46°31′N, 6°36′E). The depth contours are in meters. The submarine tracks on 20 January (runs A marked by dashed lines) and 22 January (runs B marked by solid lines) are indicated on scale. The dotted line indicates the CTD transects. The location of the ADCP is shown by a star.

an underwater radio link to a 12-m mother vessel that carries a global positioning system (GPS). The submarine tracks over the ground are recovered and plotted after dives, giving the submarine's horizontal position to within about 2 m and its speed over the ground to within 0.5 cm s^{-1}. The submarine's echo-sounder roll and notes of heading, height above the bottom, and visual observations (e.g., whether the bottom can be seen) taken at 2-min intervals show that measurements are within 2-m distance to the boundary. Initially, the submarine descends in free fall at nearly constant speed due to predetermined negative buoyancy down to the desired depth with all motors turned off. The temperature and the pressure data are recorded during this period. This allows simultaneous intercalibration of temperature sensors in situ and measurement of mean temperature profile.

The submarine tracks and their direction corresponding to the recorded ''runs'' are shown in Fig. 1 by lines and arrows and are summarized in Table 1. Submarine temperature observations were supplemented by conventional profile measurements taken from a surface boat along a trajectory indicated by the dotted line in Fig. 1 using a lowered OTS 1500 conductivity, temperature, depth sensor (CTD), built by Meerestechnik Electronic. An upward looking bottom-mounted acoustic Doppler current profiler (ADCP; manufactured by RDInstruments), which was placed in the study area in 43-m water depth (*see Fig. 1*), provided background information on the mean currents. The workhorse, broadband ADCP recorded current profiles with 5-m bin resolution with a system frequency of 300 kHz, and continuous recording was averaged over 5-min intervals.

Table 1. The submarine tracks. The third column, *z*, is the average depth of the submarine. The fourth column is the sampling frequency of thermistors on the vertical array. The fifth column is the mean submarine speed. When there are no comments, the track is crosswind and in the epilimnion. Runs labeled A are in period A when $L = -1$ m and $D = 75$ m. Runs labeled B have $L = -12.5$ m and $D = 120$ m.

Run	Date (1998)	*z* (m)	Frequency (Hz)	Speed (m s^{-1})	Comments
A3	20 Jan	8.7 ± 0.53	10	0.52	downwind
A9	20 Jan	81.8 ± 0.46	10	0.50	in the thermocline
A10*	20 Jan	55.6 ± 0.69	10	0.50	
B2	22 Jan	9.1 ± 1.60	30	0.47	downwind
B6*	22 Jan	28.9 ± 0.56	10	0.47	
B8*	22 Jan	29.1 ± 1.60	10	0.50	downwind
B10*	22 Jan	82.7 ± 1.40	10	0.50	
B11*	22 Jan	48.6 ± 0.31	10	0.50	

* The track interacts with the cold slope boundary layer.

Fluctuations in submarine motion

The submarine maintained depth constant to ±0.85 m during each run, with a typical standard deviation of 0.5 m. The deviations from the heading angle were typically ±3.1°. Typical fluctuations in pitch and roll were ±0.3° and ±0.8°, respectively. The dominant undulations are due to the pilot's adjustments to hold constant depth and heading and had periods of about 1.5 min. This period is much longer than the periods corresponding to the frequencies used in mixing parameter estimations and has a negligible effect on the present analysis.

Roll and pitch movements appear to be coherent at the wave number of 47 cycles per meter (cpm), corresponding to a horizontal scale of 13 cm and a period of 0.26 s, with a phase difference of 160°. At the same wave number a small, but barely significant, coherence peak is found between the temperature recorded by the upper and lower sensors of the vertical array (0.38 ± 0.2 and 0.26 ± 0.05 for runs A and B, respectively). This may be a consequence of the noise generated by the propeller at a period of 0.3 s. The

energy estimates in the ensemble-averaged temperature spectra show a slight peak at that wave number whose magnitude is always less than the width of the confidence interval (Fig. 3a).

Currents and the observed thermal structure

The measurements were made on 20 and 22 January 1998 and are referred to as periods A and B, respectively. Dives started around 0900 h and lasted until midafternoon. At this time of the year, air temperatures are typically below water temperatures providing for lake cooling. The lake remains weakly stratified, with a seasonal thermocline in the depth range of about 100 m. Currents in the near-shore area where this study was carried out are always shore parallel. Depth averaged mean current for the 2 d is about 4.5 ± 1.8 cm s^{-1} with approximately westward direction along the shore. Vertical shear estimated from the ADCP profiles remains low (shear^2 O[10^{-6} s^{-2}]) and almost homogeneous throughout the water column during period A. This value is close to the one observed by Lombardo and Gregg (1989) during their study of the convective oceanic boundary layer and indicates that turbulent production by shear is not important. We do not observe the diurnal changes in the shear that were reported by Lombardo and Gregg. The effect of winds during period B leads to an increase of the shear to O(10^{-4} s^{-2} for shear^2) in the upper 30 m while it remains on the same level as on period A below that depth.

Figure 2 shows the temperature distribution derived from CTD casts at the site. For A (Fig. 2a) the weather was calm with some light snowfall. For B (Fig. 2b) the sky was overcast with the wind blowing almost directly offshore from the northeast at about 8 m s^{-1}. On both days the air temperature was close to 0°C, well below the lake surface temperature of about 7°C. Mean surface heat fluxes from surface waters to the atmosphere, H, over the measurement periods are 55 ± 11 W m^{-2} and 105 ± 20 W m^{-2} for A and B, respectively. Hereinafter the standard deviation will be indicated using the $\pm$ sign. The Monin-Obukov length scale, L, characterizes the distance from the surface where the wind stress and the buoyancy are equally effective in producing turbulence and is defined as $L = -u_*^3/\kappa B_0$, where $B_0 = -g\alpha H/C_P\rho$ is the surface buoyancy flux. The gravitational acceleration is g, the coefficient of thermal expansion is α, the net surface heat flux is H, the specific heat of water is C_P, and the density of water is ρ. $\kappa = 0.4$ is the von Karman's constant and u_* is the friction velocity in the water estimated by supposing that the wind stress is balanced by the stress on the water surface. During runs A and B, the Monin-Obukov length scale, L, was approximately -1 m and -12.5 m, respectively. Meteorological data used in the calculations of B_0 and L were obtained from a station located close to the site. Uncertainties in the values of B_0 and L are derived from the errors in calculating the net surface heat flux, H, and the friction velocity, u_*, and are estimated to be 10% and 15%, respectively. Errors in calculating H include the errors in measuring air and surface water temperature, the wind speed, and the shortwave radiation. The errors in u_* result from errors in measuring the wind speed and calculating the drag coefficient.

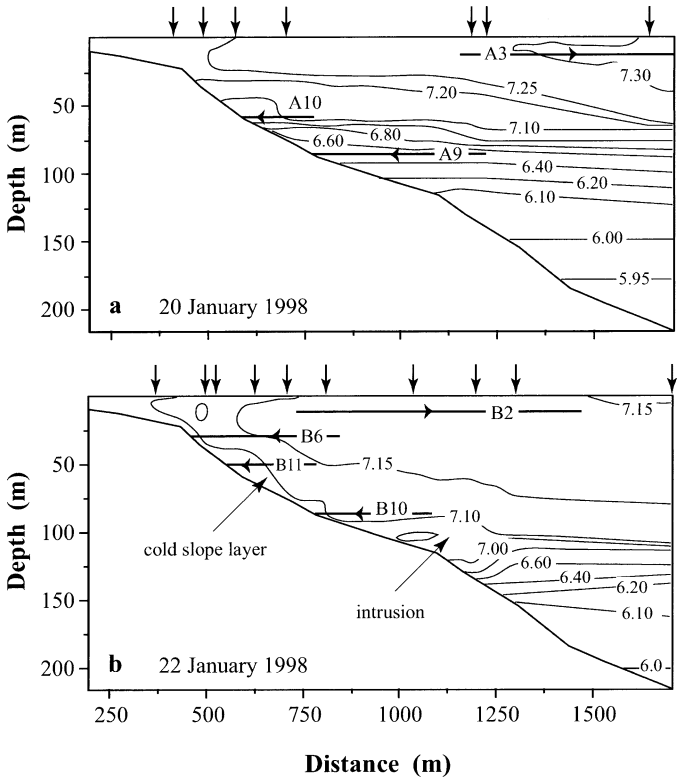

Fig. 2. Isotherm contours derived from CTD sections made over the sloping side of lake (a) on the afternoon of 20 January and (b) on the morning of 22 January. Temperatures are in °C. The vertical scale is the depth, and the horizontal scale is the distance from shore. The location of the CTD profiles is indicated by vertical arrows. The tracks of the submarine for different runs are marked on the figure by horizontal lines to scale, with the arrows indicating the direction. The cold slope layer and its intrusion into the thermocline is shown in (b). Note that there is also evidence of colder water (e.g., 7.10°C) on the slope in (a).

The buoyancy frequency, N, defined as $N^2(z) = g\alpha(dT/dz)$, in the thermocline (below a mixed layer depth, D, of about 75 m and 120 m for A and B) is about 6.5×10^{-3} s^{-1} on both days. Here, g is the acceleration of gravity, α is the coefficient of thermal expansion, and z is the depth. Except near the surface, the epilimnion is weakly, but stably stratified. In the epilimnion, the horizontal temperature gradient is observed to be greater in A than in B, with temperature increasing in the offshore direction (0.39 and 0.056 mK m^{-1}, respectively, compare Fig. 2a,b).

During periods of winter convection, the temperature of the water overlying the shallow, typically 2–5 m deep, shelf region around the edge of Lake Geneva falls more rapidly than that over deeper water. This causes spilling or cascading of relatively dense water from the shallow down the sloping sides of the lake in the form of gravity currents, typically 2–15 m thick and 0.1 K lower in temperature than the overlying water. This cascade is observed to have a mean downslope speed of $U = 0.05$ m s^{-1}, on the 5–20° lateral slopes of the lake at depths shallower than that of the thermocline (Fer et al. 2000, 2001). Figure 2b provides an example of a

cold layer flowing downslope as gravity current and intruding into the thermocline at about 1200 m from shore.

The submarine tracks are shown in Fig. 1b and are indicated in Fig. 2 by horizontal, constant-depth lines, with arrows showing their directions. Among the runs propagating toward the lateral slope, A9 is in the thermocline. Runs A10, B6, B10, and B11 enter the cold slope boundary layer. Statically unstable regions, where cold water lies above warmer water, can be seen near the surface. Earlier analysis of the data suggests that the horizontal scale of convective plumes in the epilimnion is about 5–6 m (Thorpe et al. 1999).

Scalar turbulence

In order to estimate mixing parameters from our temperature data, we shall rely on several well-established concepts. For a scalar quantity, here temperature, in a turbulent field the spectrum of gradient fluctuations in one dimension can be represented by the Batchelor form (Gibson and Schwarz 1963)

$$S(k) = (q/2)^{1/2}\chi k_B^{-1}K_m^{-1}f(k) \tag{1}$$

where k is the wave number in units of cpm (we shall use the horizontal wave number), $q \approx 3.4$ (Dillon and Caldwell 1980) is a universal constant related to the least principal rate of strain of the velocity spectrum, K_m is the molecular diffusivity of heat, χ is the rate of dissipation of temperature variance, and $k_B = (\varepsilon\nu^{-1}K_m^{-2})^{1/4}$ is the Batchelor wave number. Here ε is the dissipation of turbulent kinetic energy and ν is the kinematic viscosity. The nondimensional spectrum can be written as

$$f(\mathrm{k}) = \mathrm{k}\left\{e^{-\mathrm{k}^2/2} - \mathrm{k}\int_{\mathrm{k}}^{\infty} e^{-x^2/2}\,dx\right\} \tag{2}$$

with the nondimensional wave number $\mathrm{k} = kk_B^{-1}(2q)^{1/2}$.

Assuming that the temperature gradient field is locally isotropic, the rate of dissipation of temperature variance, χ, is given by

$$\chi = 6K_m\int_0^{\infty} S(k)\,dk = 6K_m\langle(\partial T'/\partial x)^2\rangle \tag{3}$$

where T' is the temperature fluctuation and the angle brackets indicate an ensemble average. Based on an assumed balance between the generation of temperature fluctuations by turbulent vertical overturns in a mean temperature gradient and its dissipation due to molecular diffusion, Osborn and Cox (1972) show that vertical eddy diffusivity, K_z, can be expressed as

$$K_z = 3K_m\frac{\langle(\partial T'/\partial x)^2\rangle}{\langle\partial T/\partial z\rangle^2} \tag{4}$$

Here, all other processes producing temperature fluctuation variance are neglected and isotropy is assumed for scales smaller than the overturns.

The universal temperature spectrum in the inertial convective range can be scaled as (Gibson and Schwarz 1963)

$$\frac{E(k)k_s^3\nu}{\chi} = \beta\left[\frac{k}{k_s}\right]^{-5/3} \tag{5}$$

where $E(k)$ is the temperature fluctuation spectrum, k is the wave number, ν is the kinematic viscosity, and $k_s = (\varepsilon\nu^{-3})^{1/4}$ is the Kolmogorov wave number. Gibson and Schwarz (1963) determined the proportionality constant β as 0.35 ± 0.05. The values of β range between 0.35 and 1.15, which introduces an uncertainty of a factor of 2 (Gargett 1985).

Assuming a stationary balance between the buoyancy flux and the dissipation of turbulent kinetic energy, ε, Osborn (1980) has proposed a scaling for vertical diffusivity of the form

$$K_z = \Gamma\varepsilon N^{-2} \tag{6}$$

where Γ is the mixing efficiency and N is the buoyancy frequency. Γ indicates the conversion efficiency of turbulent kinetic energy into potential energy of the system.

A range of estimates of Γ is found and used in the literature. Lilly et al. (1974) obtained $\Gamma = 0.33$ from atmospheric measurements. Weinstock (1978) proposed that $\Gamma = 0.8$ on theoretical grounds. Oakey (1982) estimated $\Gamma = 0.259 \pm 0.21$ using dissipation rate calculations from the high wave number cutoff of the temperature microstructure spectra from oceanic waters. Recently, Greenspan et al. (2001) have proposed $\Gamma = 0.26$ in a weakly stratified mixed layer. Zülicke et al. (1998) obtained $\Gamma = 0.22$ related to a coastal jet in the Baltic Sea, in stratified summer conditions. Ravens et al. (2000) reported an average value of $\Gamma = 0.16 \pm 0.11$ in Lake Baikal, while Gloor et al. (2000) observed $\Gamma = 0.15 \pm 0.04$ in the upper pycnocline of Lake Alpnach, both comparable to the value found in the ocean interior.

Isotropy and estimation of mixing parameters, ε, K_z, and χ

We can assess the degree of isotropy from the shortest separation of the temperature sensors (0.24 m) to the longest (1.68 m) by comparing the root mean square (rms) temperature fluctuation gradients over equal vertical and horizontal scales. The records are transformed into wave number space by making the Taylor hypothesis and using the submarine speed through the water, 0.5 ± 0.02 m s^{-1}. Typical values of the ratio $r = \langle(\partial T'/\partial x)^2\rangle/\langle(\partial T'/\partial z)^2\rangle$ for 0.24 m and 1.68 m separations are 1.03 ± 0.05, 1.23 ± 0.17 for near-surface tracks, 1.12 ± 0.2, 1.4 ± 0.5 for near-slope zones, and 0.91 ± 0.1, 1.05 ± 0.33 for deeper waters away from the slope, respectively. The values of r close to one suggest that the temperature fluctuation field is nearly isotropic at scales less than about 1.68 m (Warhaft 2000). For run A9, which is in the thermocline (Table 1), we find $r = 0.3 \pm 0.2$.

Another estimate of isotropy can be obtained from the buoyancy Reynolds number, $\mathrm{Re}_\rho = \varepsilon N^{-2}\nu^{-1}$. When Re_ρ is greater than 30, isotropy is likely (Istweire et al. 1993; Sander et al. 2000). Using the results shown later, the estimated values of εN^{-2} change between 10^{-4}–10^{-2} m^2 s^{-1}, for open waters (Fig. 6a), and 10^{-5}–10^{-3} m^2 s^{-1} for near-slope region (Fig. 6b). With the viscosity of fresh water $\nu = \mathrm{O}(10^{-6})$ m^2 s^{-1}, the range $10^2 < \mathrm{Re}_\rho < 10^4$ is observed for open waters

and $10^1 < \mathrm{Re}_\rho < 10^3$ in the near-slope region. From the above calculations we conclude that we can use Eqs. 3 and 4 with some confidence. The assumption of isotropy becomes rather doubtful in the thermocline. For run A9 with $N \sim 6.5 \times 10^{-3}$ s^{-1} and ε of the order of 10^{-11} m^2 s^{-3} (Fig. 4a) Re_ρ is about 0.2.

Data acquired on each submarine run are divided into eight equal-sized segments, and temperature fluctuations are calculated after linearly detrending the data. The resulting segment lengths of about 100 m (about 6,000 data points for each of the six sensors recording in parallel) for 10-m depth tracks allowed estimates to be made over a large enough length to minimize the effects of individual plumes. Segment lengths of 20–50 m (about 1,000 data points for each sensor) for tracks propagating toward the slope were sufficient to resolve the transition from open waters to the near-slope zone. From free fall experiments with the submarine and from CTD profiles taken in the area, weak and nearly linear vertical temperature gradients were observed in the depth range of operation. Therefore, vertical temperature gradients are derived from the data recorded by the top and bottom sensors with vertical separations of 1.2 and 1.68 m for runs A and B, respectively.

The temperature data from the sensor at the level of the pressure sensor recording the submarine depth are transformed into horizontal wave number space and are used in calculations of $\partial T'/\partial x$, giving a horizontal spatial resolution of 1.5 and 5 cm for 30 and 10 Hz sampling frequencies, respectively. The rate of dissipation of the temperature variance, χ, is then estimated from calculating the variance of $\partial T'/\partial x$ using Eq. 3 and taking the molecular diffusivity of heat at 7°C, $K_m = 1.38 \times 10^{-7}$ m^2 s^{-1}. As can be seen from the nondimensional temperature gradient spectrum shown in Fig. 3b, the spectral values reach to the peak of the spectrum and approximately 50% of the variance is resolved. The model Batchelor spectrum is used in calculations of χ to account for the values missing beyond the peak.

Spectra of temperature fluctuations and temperature fluctuation gradients of each run are calculated for each of the six sensors and then ensemble averaged. This provides for sufficient averaging in order to fulfill the conditions of spatial and temporal homogeneity at the mean submarine depth. The ensemble-averaged spectra are subsequently band averaged over 10 values for $k \leq 30$ cpm and over 20 values for $k > 30$ cpm. The dissipation rate of kinetic energy, ε, is estimated from these temperature fluctuation spectra where the portion of the power spectra corresponding to the inertial convective subrange is identified with a best-fit line. The Kolmogorov wave number, k_s, is calculated from Eq. 5 using the known value of χ. The dissipation rate of kinetic energy is then estimated as $\varepsilon = k_s^4 \nu^3$, with $\nu = 1.43 \times 10^{-6}$ m^2 s^{-1} (viscosity of fresh water at 7°C). The vertical eddy diffusivity, K_z, is estimated from Eq. 4, after obtaining $\partial T/\partial z$ from top and bottom sensors of the vertical array.

Results

The ensemble-averaged temperature fluctuation spectrum derived from all six sensors is illustrated in Fig. 3a for run B2 (~10-m depth) in open waters. The −5/3 inertial subrange can be clearly identified. The spectral energy level of B2 is about half a decade higher than that of run A3 (not shown) at the same depth. This can be explained by the higher energy input from the wind on 22 January, which possibly increased the temperature variance. During runs A and B, the Monin-Obukov length, L, was approximately −1

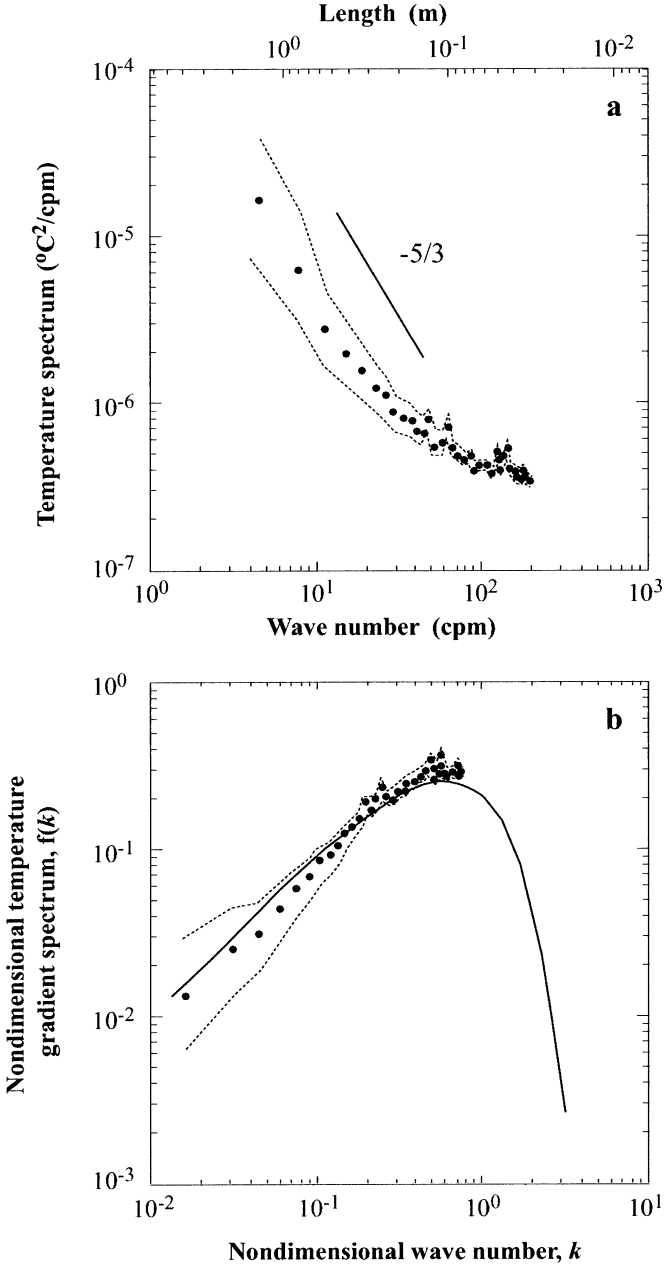

Fig. 3. (a) Ensemble-averaged spectrum of temperature fluctuations for run B2. The line of −5/3 slope represents inertial convective subrange (Eq. 5). (b) Ensemble-averaged nondimensional spectrum of temperature gradient, f(k), for the run B2. Solid curve is the Batchelor spectrum. The values of ε and χ used in the calculation of the spectra were 4.8×10^{-9} m^2 s^{-3} and 7×10^{-7} °C^2 s^{-1}, respectively. The spectra are presented with 10 data points band averaged for $k \leq 30$ cpm and 20 data points for $k > 30$ cpm. The dashed envelopes show the 95% confidence intervals, accordingly.

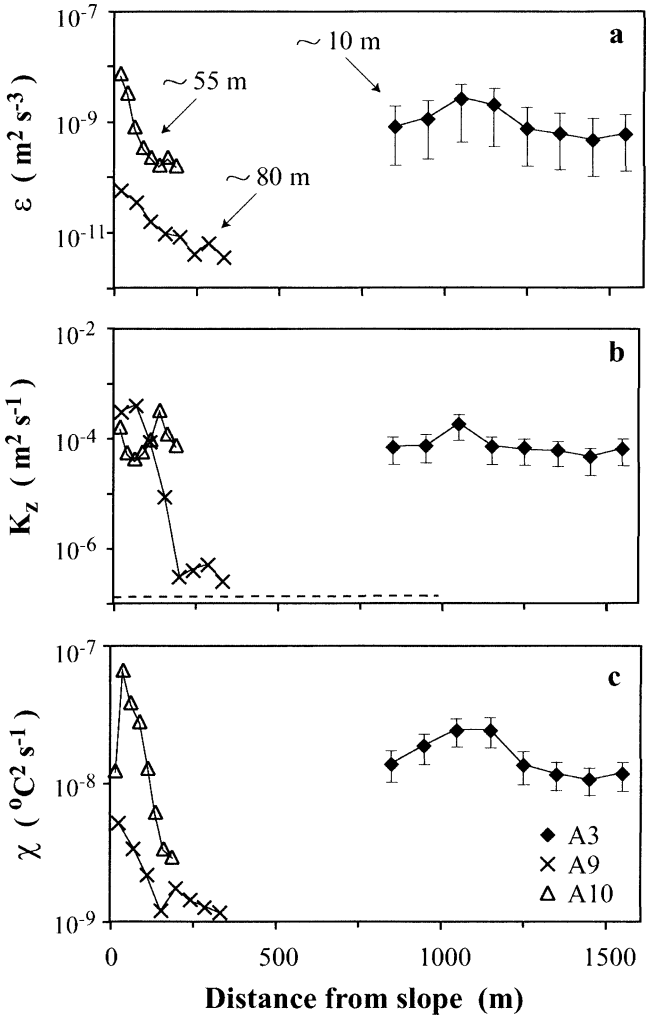

Fig. 4. Horizontal distribution of estimated values of (a) ε, (b) K_z, and (c) χ under calm conditions on 20 January, period A, for the runs A3, A9, and A10. The horizontal axis is the distance from the slope, normal to mean isobaths. Only error bars for run A3 are shown. The dashed line in (b) is the molecular diffusivity of heat at about 7°C, $K_m = 1.38 \times 10^{-7}$ m^2 s^{-1}.

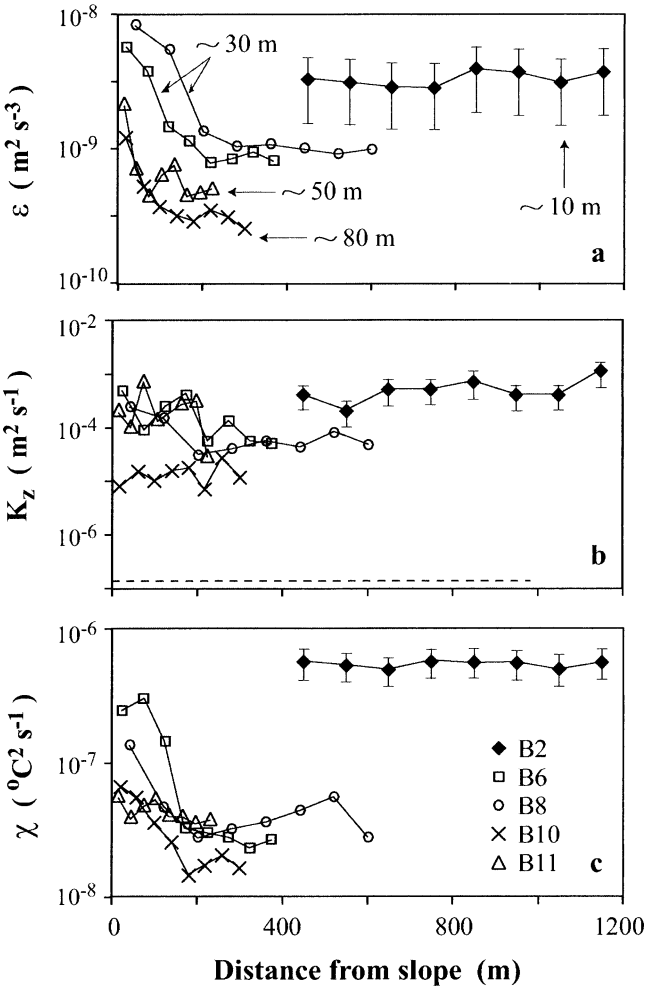

Fig. 5. Horizontal distribution of estimated values of (a) ε, (b) K_z, and (c) χ under windy conditions on 22 January, period B, for the runs B2, B6, B8, B10, and B11. The horizontal axis is the distance from the slope, normal to mean isobaths. Only error bars for run B2 are shown. The dashed line is as in Fig. 4b.

m and -12.5 m, respectively, leading to $D/-L$ ratios of 75 and 8. Here, D is the mixed layer depth. Free convection (independent of mechanical mixing at water surface) is established below a depth of $-2L$ (Shay and Gregg 1986) if $D/-L \gg 1$. We may therefore expect that run B2 is affected by the wind stirring, whereas A3 is dominated by free convection. Under the free convective conditions of period A, the low wave number portion of the temperature spectrum is likely to be affected by the presence of convective plumes. A peak at a wave number corresponding to a scale of ~5 m observed in the spectra of run A3 but not seen in those of B2 is consistent with the horizontal scale of observed plumes (Thorpe et al. 1999).

The ensemble-averaged temperature gradient spectrum calculated for run B2 is nondimensionalized by $(q/2)^{1/2}\chi k_B^{-1}K_m^{-1}$ and shown as a function of nondimensional wave number, k in Fig. 3b. The spectrum agrees fairly well with the Batchelor form represented by the solid curve. This is different from Dillon and Caldwell (1980), who had reported a strong deviation from the Batchelor shape in the low wave number portions for Cox numbers $Cx = \langle(dT'/dz)^2\rangle/\langle dT/dz\rangle^2$ lower than 500, indicating that turbulence is weak compared to stratification. In our observations Cx changes in the range $20 < Cx < 1{,}000$. The values of ε and χ used in the calculation of the spectra are 4.8×10^{-9} m^2 s^{-3} and 7×10^{-7} °C^2 s^{-1}, respectively. The corresponding Batchelor and Kolmogorov wave numbers are $k_B \sim 600$ cpm and $k_s \sim 200$ cpm, respectively.

Figures 4 and 5 illustrate the horizontal distribution of ε, K_z, and χ along the submarine tracks for periods A and B, respectively. The errors are principally derived from the uncertainties in β, temperature resolution, spatial temperature fluctuation gradients, and finding k_s. The uncertainties are about 25% and 50% for χ and K_z, respectively. Greater uncertainties arise for ε. A systematic error of 10% in finding k_s alone results in a 40% error in ε. Consideration of accuracy and assumption of isotropy may introduce an error of 50% into the values of ε. As a result, ε can be estimated to

within a factor of 2. While this level of uncertainties in the present study may seem high, it has to be realized that it is comparable to that of other microstructure studies in oceans and lakes. It should also be noted that the conclusions of this study are based on variations in ε, K_z, and χ that largely exceed the level of uncertainties. For clarity, only error bars for runs A3 and B2 far from the slope at about 10-m depth are shown.

It can be observed that the estimated values of all parameters increase by 1 to 3 orders of magnitude within a 150-m horizontal distance from the slope (runs A9, A10, B6, B8, B10, and B11). The values of ε estimated for B2 are approximately one order of magnitude greater than those of A3, probably a consequence of higher surface buoyancy flux and smaller z/L during period B. At greater depths, smaller values of the mixing parameters are obtained in the portions distant from the sloping boundary. The vertical eddy diffusivity values in the thermocline, run A9, which are shown for comparison, are close to the coefficient of molecular diffusivity (indicated by dashed lines on Figs. 4b and 5b), suggesting that little heat flux occurred at those depths, off the slope. There is, however, still an increase in all mixing parameters at that depth as the slope is approached. The χ estimates at distances far from the slope show more homogeneity with depth in period A than on runs B. They are approximately of the same order of magnitude with variations within the error limits. Near the slope, χ increases by up to two orders of magnitude.

Although probability density functions (PDFs) of ε and χ in homogeneous turbulence are lognormal, they do not fully fit the lognormal shape in oceans and in lakes (Gregg 1987; Alford and Pinkel 2000; Sander et al. 2000). Discrepancies are attributed to instrumental noise and intermittence, as well as depth dependency of the parameters flattening the distribution. Statistical properties of log ε and log χ have been calculated covering all our observations. The PDFs are reasonably lognormal. The mean value, standard deviation, skewness, and kurtosis values derived over all estimations yield -9.2, 0.88, -0.05, and 1.2 for log ε and -8.3, 0.39, 0.95, and 1.7 for log χ, respectively. For the near slope estimates, the PDFs are skewed to larger values, indicating again that the dynamic in this layer is different from that in the open waters.

The detailed investigation in the lateral boundary layer dynamics (Fer et al. 2001), which we have carried out in parallel, provides for an opportunity to estimate the dissipation values within that layer by local parameters. This cold boundary layer is typically 2–15 m thick, and the law-of-the-wall may be applied to it. For smooth flow over the fine sediments in lakes and oceans, the value of ε close to the slope can be investigated. According to the law-of-the-wall, ε as a function of mean flow, U, scales as $\varepsilon = u_*^3/\kappa z$, where $\kappa = 0.4$ is the von Karman constant, z is the vertical distance from the wall, and u_* is the friction velocity, which scales as $u_* = C_D^{1/2}U$. Here C_D is the drag coefficient. Introducing typical observed values of $C_D = 4.5 \times 10^{-3}$ and the mean downslope flow associated with the cascade $U = 0.05$ m s^{-1} (Fer et al. 2001), a value of $\varepsilon = 9 \times 10^{-9}$ m^2 s^{-3} can be calculated for $z = 10$ m from the slope. At $z = 1$ m, ε is about 8×10^{-8} m^2 s^{-3}. With the bottom slope of $\sim 10°$,

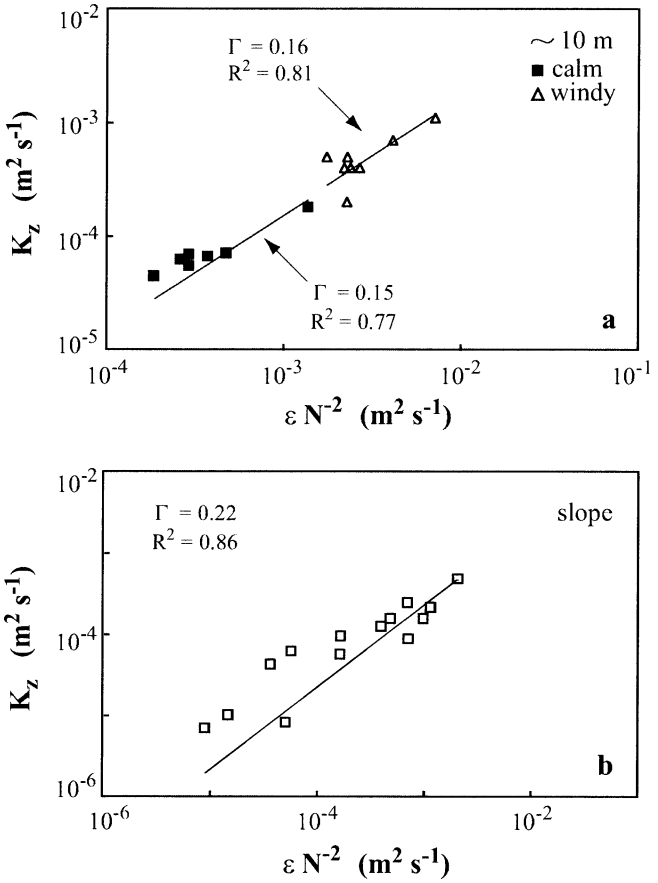

Fig. 6. Scatter plots of εN^{-2} versus K_z for runs (a) 10-m runs of windy and calm conditions and (b) near-slope region. The best-fit regression lines with intercept set to zero are indicated. The mixing efficiency, Γ, and R^2 values are indicated on the figure.

vertical distance of 1–10 m corresponds to approximately 6–60 m horizontal distance from the slope. These values are close to the ones estimated near the slope from the submarine study (Figs. 4a and 5a). The elevated values of ε at considerable horizontal distances from the slope (100–150 m) may be attributed to the submarine tracks crossing the downslope flow obliquely (Fig. 1).

For a check on the consistency of the dissipation and temperature dissipation rates obtained from present horizontal observations with vertical microstructure measurements, the mixing efficiency, Γ, has been obtained from Eq. 6 using the estimated values of ε, K_z, and N. Although the water column was weakly stratified, there was sufficient stratification to measure both ε and K_z as well as the mean gradients to estimate Γ. Best-fit values of Γ in the surface layers are 0.15 $\pm$ 0.1 and 0.16 $\pm$ 0.1 for runs A3 and B2 respectively (Fig. 6a), whereas $\Gamma = 0.22 \pm 0.2$ is obtained from all the runs shown in Figs. 4 and 5 within 150 m horizontally of the slope (Fig. 6b), except A9, which is in the thermocline. These values are within the range of estimates given in the literature.

In order to determine the importance of convective cooling during the study periods, similarity scaling in the mixed layer (''convective scaling'') is applied to ε and χ estimates

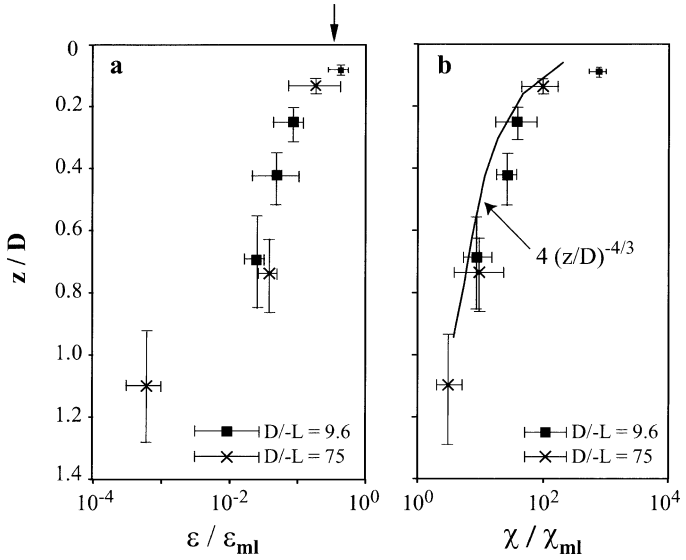

Fig. 7. Profiles of average (a) $\varepsilon/\varepsilon_{ml}$ and (b) χ/χ_{ml} normalized according to convective mixed layer scaling. Only the portions of data far from the slope are used. The vertical axis is the depth normalized by the mixed layer depth, $D \sim 75$ m and $D \sim 120$ m for runs A and B, respectively. Horizontal error bars represent the minimum and maximum values derived for each z/D, while vertical error bars are uncertainties in z/D. $D/-L$ ratios are indicated on the figure with corresponding horizontal error bars showing the relative error in (a) $\varepsilon/\varepsilon_{ml}$ and (b) χ/χ_{ml}. The arrow in (a) shows the value found by Shay and Gregg (1986) in the open ocean convective layer. The curve in (b) is proposed by Brubaker (1987).

far from the slope following the suggestions by Brubaker (1987) for χ and Lombardo and Gregg (1989) for ε. Characteristic similarity scales in the mixed layer are $\varepsilon_{ml} = B_0$ for ε and $\chi_{ml} = w_* \theta_*^2/D$ for χ, where $w_* = (DB_0)^{1/3}$ is the velocity scale and $\theta_* = H/\rho C_p w_*$ is the temperature scale. B_0 is the surface buoyancy flux, D is the mixed layer depth, C_p is the specific heat of water, taken as 4,200 J(kg °C)$^{-1}$, and ρ is the density of water. The convective time scale, D/w_*, is 3.4 ± 1 and 3.1 ± 0.4 h for periods A and B, respectively. Therefore, a quasi-equilibrium state of mixing with plumes to depth D is reached approximately 3–4 h after the nocturnal cooling started.

Figure 7 shows the profiles of $\varepsilon/\varepsilon_{ml}$ and χ/χ_{ml}, obtained from portions of data far from the slope with respect to normalized depth, z/D. At $z/D \sim 0.2$, the normalized dissipation rate has a value close to that found by Shay and Gregg (1986) in the open ocean convective layer, where $\varepsilon/\varepsilon_{ml} \approx 0.6$ was reported. Even though shear^2 during period B was O(10^{-4} s^{-2}), ε did not increase to 10 similarity scales as observed by Lombardo and Gregg (1989). This indicates that wind shear is not sufficiently important to affect the convective regime at 10-m depth. Below that depth, in $0.3 < z/L < 1$, $\varepsilon/\varepsilon_{ml}$ appears to fall off more rapidly than in the ocean (Shay and Gregg 1986; Lombardo and Gregg 1989) or in the atmosphere (Kaimal et al. 1976). We do not resolve the sharp falloff near $z/D = 1$. However, the last value in the profile at $z/D \approx 1.1$ is significantly smaller than the values at $z/D \approx 0.7$, and a sharp reduction around $z/D = 1$ can be expected. Shay and Gregg observed a more rapid decay with depth similar to ours in the case of a temperature gradient in the upper layer. The χ/χ_{ml} profile (Fig. 7b) lies near the curve proposed by Brubaker (1987) for the convective boundary layer in lakes. Lombardo and Gregg (1989) had confirmed that the convective scale also works well in the ocean away from the near-surface layer. The actual values of χ that we observe are in the same range as Brubaker's and show a similar decrease with depth in the open waters.

Discussion and conclusions

The dominant mixing processes in oceans and lakes differ according to a variety of factors, including stratification and proximity to boundaries. Mixing occurring in the epilimnion and thermocline is greatly influenced by thermal exchange with the atmosphere, by wind driven mixing (e.g., breaking waves and Langmuir circulation) generated at the surface, and by turbulence induced by shear resulting from, for example, internal waves (Imberger and Hamblin 1982; Spigel et al. 1986; Gregg 1987).

Ivey and Imberger (1991) categorize turbulence in a stratified fluid according to two dimensionless variables, an overturn Froude number, Fr_T, and an overturn Reynolds number, Re_T. These are defined as $\mathrm{Fr}_T = [\varepsilon/(g'^{3/2}L_C^{1/2})]^{1/3}$ and $\mathrm{Re}_T = \varepsilon^{1/3}L_C^{4/3}/\nu$, where g' is a reduced acceleration of gravity, ν is the kinematic viscosity, and L_C is an overturn length scale, which is close to the Thorpe length scale, L_T (Dillon 1982; Ivey and Imberger 1991). A maximum in mixing efficiency is found at $\mathrm{Fr}_T = 1$. Values of $\mathrm{Fr}_T > 1$ indicate a mixing mechanism where the dissipation exceeds the available potential energy contained in the overturn events, while for $\mathrm{Fr}_T < 1$ potential energy is predominantly balanced by the kinetic energy fluctuations, as in the case of internal waves or intrusions. The state of turbulence in a stratified fluid may thus be inferred from a Fr_T-Re_T diagram.

The scale, L_T, is a statistical measure for the vertical size of overturning eddies. To estimate L_T, a density profile is reordered to restore monotonicity and hence static stability. The Thorpe scale can then be calculated as the rms of the nonzero displacements, the distance over which each parcel has to move to obtain the monotonic profile. From the time series recorded by the vertical array of sensors, temperature-depth profiles are obtained in a range spanning 0 to 1.68 m relative to the submarine depth. By rearranging the data, displacements are calculated with minimum and maximum limits of 0.24 m and 1.68 m (1.2 m for A files) and L_T is estimated as their rms value. Extensive analysis of L_T in Lake Geneva was carried out by Zhang (1994). Apart from some episodic events, long-term (several years) mean values were typically in the order of 1 m during winter in the upper 80-m layer. There is also a certain tendency for values to drop down when approaching the shore (from 6 km offshore to 1 km offshore). Therefore, displacements calculated over 0.24–1.68 m are representative, and we use L_T estimates with some confidence. The temperature difference, ΔT, between the top and bottom sensors gives an estimation of the density anomaly, and the reduced acceleration of gravity can be calculated by $g' = g\alpha\Delta T$, where α is the coefficient of thermal expansion taken as 4.6×10^{-5} °C^{-1} for fresh water at 7°C.

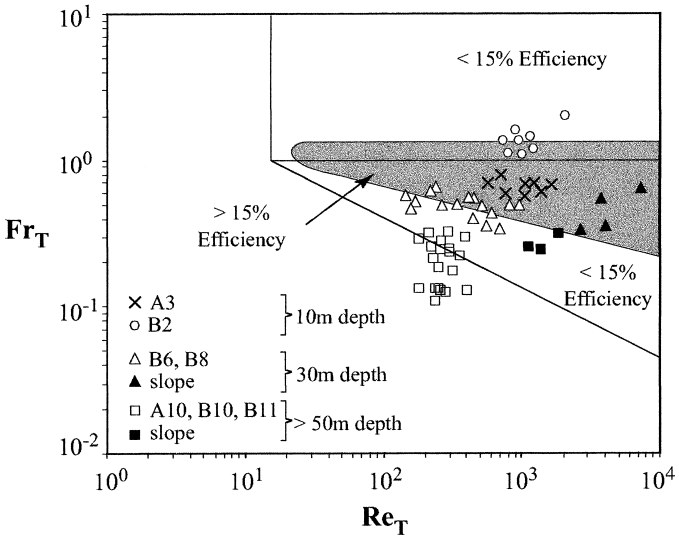

Fig. 8. The overturn Froude number, Fr_T, versus Reynolds number, Re_T, diagram showing the various flow regimes. The limiting lines and the shaded area of high mixing efficiency are given by Ivey and Imberger (1991). Points derived from measurements within 150 m horizontally of the slope are shown as solid black symbols. There is a trend toward higher mixing efficiency as the slope is approached.

The dimensionless overturn Froude and Reynolds numbers are calculated from the estimated values of ε, L_T, and g', and the data are plotted in the Re_T-Fr_T diagram in Fig. 8. The gray shaded area marks the high mixing efficiency zone given by Ivey and Imberger (1991).

There is a clear distinction in the diagram between the data of different days and different locations. Near 10-m depth, the values calculated for the windy day, B2, show more activity than those of the calm day, A3, and lie in the range found by Ivey and Imberger (1991) to characterize wind-induced mixing ($Re_T = 10^2$ to 10^4 and $Fr_T = 1$ to 10). The points derived from measurements within 150 m horizontally of the slope agree with other boundary-mixing observations reported by Imberger and Ivey. The active mixing in the near-surface layer and the near-slope layer is distinguished in the diagram from that in the relatively calm deeper layers. The relatively calm deeper layer values cluster in a separate group, and mixing in the slope boundary layer at comparable depths is higher.

The observations from a submarine highlight some of the mixing processes over the sloping sides of Lake Geneva during weak winter stratification. It would have been more difficult to obtain the same information by conventional profiling techniques. The horizontal profiles allow distinctions to be made between the slope boundary layer and off-slope waters at similar depths using identical sampling and analysis techniques. The mean dissipation rate per unit mass averaged over the epilimnion varies between $O(10^{-10})$ m^2 s^{-3} in calm weather to $O(10^{-8})$ m^2 s^{-3} in winds of 8 m s^{-1}, compared to surface buoyancy fluxes of 6×10^{-9} m^2 s^{-3} and 1.1×10^{-8} m^2 s^{-3}, whereas near the slope it has an average value of 3×10^{-8} m^2 s^{-3}.

The shallow off-slope waters have ε and χ values with similarity scaling comparable to that in the open ocean and in lakes during strong summer nighttime cooling (Fig. 7). Although in $0.3 < z/D < 1$, ε is found to decay with depth more rapidly than expected, the overall features of a convective boundary layer are documented. The slope boundary layer has different mixing characteristics. The values of K_z and ε are an order of magnitude greater than those observed in off-slope waters at the same depth and are distinct in the Re_T-Fr_T diagram. However, unlike the summer stratified conditions in which boundary mixing is induced by internal wave activity or along-slope currents, mixing in the slope boundary layer studied here is related to the presence of winter cascading, gravity currents carrying cold water downslope. Estimates of the mixing efficiency, Γ, are consistent with those reported by others. Near the slope, even in deeper layers, Γ is found to be comparable to values obtained both for windy and strongly convective conditions of surface waters. This and the gradual decay in ε suggest that the dynamics of the main body of water in the vicinity of the slope may be strongly influenced by near-slope mixing processes during periods of winter cooling.

References

ALFORD, M., AND R. PINKEL. 2000. Patterns of turbulent and double-diffusive phenomena: Observations from a rapid profiling microconductivity probe. J. Phys. Oceanogr. **30:** 833–854.

BRUBAKER, J. M. 1987. Similarity structure in the convective boundary layer of a lake. Nature **330:** 742–745.

DILLON, T. M. 1982. Vertical overturns: A comparison of Thorpe and Ozmidov length scales. J. Geophys. Res. **87:** 9601–9613.

———, AND D. R. CALDWELL. 1980. The Batchelor spectrum and dissipation in the upper ocean. J. Geophys. Res. **85:** 1910–1916.

ERIKSEN, C. C. 1998. Internal wave reflection and mixing at Fieberling Guyot. J. Geophys. Res. **103:** 2977–2994.

FER, I., U. LEMMIN, AND S. A. THORPE. 2000. The winter cold slope boundary layer, p. 301–305. In Proceedings of Fifth IAHR international symposium on stratified flows.

———, ———, AND ———. 2001. Cascading of water down the sloping sides of a deep lake in winter. Geophys. Res. Lett. **28:** 2093–2096.

GARGETT, A. E. 1985. Evolution of scalar spectra with the decay of turbulence in a stratified fluid. J. Fluid Mech. **159:** 379–407.

GIBSON, C. H., AND W. H. SCHWARZ. 1963. The universal equilibrium of turbulent velocity and scalar fields. J. Fluid Mech. **16:** 365–384.

GLOOR, M., A. WÜEST, AND D. M. IMBODEN. 2000. Dynamics of mixed bottom boundary layers and its implications for diapycnal transport in a stratified natural water basin. J. Geophys. Res. **105:** 8629–8646.

GOUDSMIT, G. H., F. PEETERS, M. GLOOR, AND A. WÜEST. 1997. Boundary versus internal diapycnal mixing in stratified waters. J. Geophys. Res. **102:** 27903–27914.

GREENSPAN, B. J. W., N. S. OAKEY, AND F. W. DOBSON. 2001. Estimates of dissipation in the ocean mixed layer using a quasi-horizontal microstructure profiler. J. Phys. Oceanogr. **31:** 992–1004.

GREGG, M. C. 1987. Diapycnal mixing in the thermocline—a review. J. Geophys. Res. **92:** 5249–5286.

IMBERGER, J., AND P. F. HAMBLIN. 1982. Dynamics of lakes, reser-

voirs and cooling ponds. Annu. Rev. Fluid Mech. **14:** 153–187.

———, AND G. N. IVEY. 1991. On the nature of turbulence in a stratified fluid. Part II: Application to lakes. J. Phys. Oceanogr. **21:** 659–680.

———, AND ———. 1993. Boundary mixing in stratified reservoirs. J. Fluid Mech. **248:** 477–491.

ISTWEIRE, E. C., J. R. KOSEFF, D. A. BRIGGS, AND J. H. FERZIGER. 1993. Turbulence in stratified shear flows: Implications for interpreting shear-induced mixing in the oceans. J. Phys. Oceanogr. **23:** 1508–1522.

IVEY, G. N., AND J. IMBERGER. 1991. On the nature of turbulence in a stratified fluid. Part I: Energetics of mixing. J. Phys. Oceanogr **21:** 650–658.

KAIMAL, J. C., J. C. WYNGAARD, D. A. HAUGEN, O. R. COTÉ, Y. IZUMI, S. J. CAUGHEY, AND C. J. READINGS. 1976. Turbulence structure in the convective boundary layer. J. Atmos. Sci. **33:** 2152–5169.

LEDWELL, J. R., AND B. M. HICKEY. 1995. Evidence of enhanced boundary mixing in the Santa Monica Basin. J. Geophys. Res. **100:** 20,665–20,679.

———, E. T. MONTGOMERY, K. L. POLZIN, L. C. S. LAURENT, R. W. SCHMITT, AND J. M. TOOLE. 2000. Evidence for enhanced mixing over rough topography in the abyssal ocean. Nature **403:** 179–182.

LILLY, D. K., D. E. WACO, AND S. I. ADELFANG. 1974. Stratospheric mixing estimated from high-altitude turbulence measurements. J. Appl. Meteorol. **13:** 488–493.

LOMBARDO, C. P., AND M. C. GREGG. 1989. Similarity scaling of viscous and thermal dissipation in a convecting boundary layer. J. Geophys. Res. **94:** 6273–6284.

MACINTYRE, S., K. M. FLYNN, R. JELLISON, AND J. R. ROMERO. 1999. Boundary mixing and nutrient fluxes in Mono Lake, California. Limnol. Oceanogr. **44:** 512–529.

OAKEY, N. S. 1982. Determination of the rate of dissipation of turbulent energy from simultaneous temperature and velocity shear microstructure measurements. J. Phys. Oceanogr. **12:** 256–271.

OSBORN, T. R. 1980. Estimates of the rate of vertical diffusion from dissipation measurements. J. Phys. Oceanogr. **10:** 83–89.

———, AND C. S. COX. 1972. Oceanic fine structure. Geophys. Fluid Dyn. **3:** 321–345.

POLZIN, K. L., J. M. TOOLE, J. R. LEDWELL, AND R. W. SCHMITT. 1997. Spatial variability of turbulent mixing in the abyssal ocean. Science **276:** 93–96.

RAVENS, M. T., O. KOCSIS, A. WÜEST, AND N. GRANIN. 2000. Small-scale turbulence and vertical mixing in Lake Baikal. Limnol. Oceanogr. **45:** 159–173.

SANDER, J., A. SIMON, T. JONAS, AND A. WÜEST. 2000. Surface turbulence in natural waters: A comparison of large eddy simulations with microstructure observations. J. Geophys. Res. **105:** 1195–1207.

SHAY, T. J., AND M. C. GREGG. 1986. Convectively driven turbulent mixing in the upper ocean. J. Phys. Oceanogr. **16:** 1777–1798.

SPIGEL, R. H., J. IMBERGER, AND K. N. RAYNER. 1986. Modeling the diurnal mixed layer. Limnol. Oceanogr. **31:** 533–556.

THORPE, S. A., P. HALL, AND M. WHITE. 1990. The variability of mixing at the continental slope. Philos. Trans. R. Soc. Lond. **A331:** 183–194.

———, U. LEMMIN, C. PERRINJAQUET, AND I. FER. 1999. Observations of the thermal structure of a lake using a submarine. Limnol. Oceanogr. **44:** 1575–1582.

TOOLE, J. M., R. W. SCHMITT, AND K. L. POLZIN. 1997. Near-bottom mixing above the flanks of a midlatitude seamount. J. Geophys. Res. **102:** 947–959.

VAN HAREN, H., N. OAKEY, AND C. GARRETT. 1994. Measurements of internal wave band eddy fluxes above a sloping bottom. J. Mar. Res. **52:** 909–946.

WARHAFT, Z. 2000. Passive scalars in turbulent flows. Annu. Rev. Fluid Mech. **32:** 203–240.

WEINSTOCK, J. 1978. Vertical turbulent diffusion in a stably stratified fluid. J. Atmos. Sci. **35:** 1022–1027.

WÜEST, A. D., D. C. VANSENDEN, J. IMBERGER, G. PIEPKE, AND M. GLOOR. 1996. Diapycnal diffusivity measured by microstructure and tracer techniques. Dyn. Atmos. Oceans **24:** 27–39.

ZHANG, S. 1994. Dynamics of vertical mixing in Lake Geneva: Overturning scales and energetics. Ph.D. thesis 1254, LRH, EPFL, Lausanne.

ZÜLICKE, C., E. HAGEN, AND A. STIPS. 1998. Dissipation and mixing in a coastal jet: A Baltic Sea case study. Aquat. Sci. **60:** 220–235.

Received: 6 July 2001
Accepted: 20 November 2001
Amended: 3 December 2001